PHYSICAL REVIEW D **109,** 103017 (2024)

# Neutron star kick driven by asymmetric fast-neutrino flavor conversion

Hiroki Nagakura[*]
*Division of Science, National Astronomical Observatory of Japan,*
*2-21-1 Osawa, Mitaka, Tokyo 181-8588, Japan*

Kohsuke Sumiyoshi[†]
*National Institute of Technology, Numazu College, Ooka 3600, Numazu, Shizuoka 410-8501, Japan*

(Received 31 January 2024; accepted 24 April 2024; published 13 May 2024)

Multidimensional nature of core-collapse supernova leads to asymmetric matter ejection and neutrino emission, that potentially accounts for the origin of neutron star (NS) kick. Asymmetric neutrino radiation fields are, in general, accompanied by large-scale inhomogeneous fluid distributions, in particular for electron-fraction ($Y_e$) distributions. Recently, it has also been revealed that lower $Y_e$ environments in proto-neutron star envelope can offer preferable conditions for collective neutrino oscillations. In this paper, we show that a dipole asymmetry of fast neutrino-flavor conversion (FFC), one of the collective neutrino oscillation modes, can power a NS kick, and that it would generate a characteristic correlation between asymmetric distributions of heavy elements in the ejecta and the direction of NS kick. We strengthen our argument for the FFC-driven NS kick mechanism by performing axisymmetric neutrino transport simulations with full Boltzmann neutrino transport. We show that this mechanism can generate linear momentum of neutrinos to account for typical proper motions of NS. Although more detailed studies are necessary, the present study opens a new channel to give a natal NS kick.

DOI: 10.1103/PhysRevD.109.103017

## I. INTRODUCTION

Main sequence stars with having masses more than $\sim 10$ times solar masses are destined to undergo gravitational collapse of the central core, and then form neutron stars (NS) or stellar-mass black holes. The released gravitational energy is mostly taken away by neutrinos, and the rest of the energy ($\lesssim 1\%$) powers ejection of materials with electromagnetic emission, generating core-collapse supernova (CCSN). The theory of CCSN suggests that explosions are, in general, asymmetric regardless of the details of mechanism, which is consistent with polarization observations [1], distributions of heavy elements in CCSN ejecta [2], and high proper velocities of NS [3] (see also references therein). Detailed insights on the inner dynamics of CCSNe can be brought by comparing theoretical models and these observations.

Observations of neutron stars embedded in supernova remnants (SNRs) exhibit that the typical proper velocity of NS is a few hundreds of km/s but some NSs have even more than a thousand km/s [3–13]. Popular scenarios to explain such high NS velocities are that the linear momentum is imparted to NS by asymmetric matter ejection [14–19] or asymmetric neutrino emission [20–25] or both [26] during the development of CCSN explosion. It should be mentioned that, when we sum up all the absolute values of neutrino momentum, it reaches $\sim 10^{43}\ \mathrm{g\,cm/s}$, while the required linear momentum for the typical NS proper motion is $\sim 10^{41}\ \mathrm{g\,cm/s}$, implying that a percent anisotropy of neutrino emission is high enough to generate NS kick. This consideration also exhibits a requirement of high precision in numerical simulations for modeling NS kick. Considerable care must be paid for the total momentum conservation in CCSN simulations; in fact, small errors can easily lead to numerical artifacts [27]. Because of the delicate problem, the self-consistent multidimensional CCSN simulations would be a unique way to quantify NS kick, and the long-term simulations may also be important, since interaction to asymmetric fallback material onto NS may also affect the proper motion (and spin) [28,29]. Finally it should also be mentioned that the NS proper motions are affected by long-term asymmetric electromagnetic emission, known as *postnatal* processes [30–33], which may need to be taken into account for comparing to observations.

In this paper, we present a new possibility that fast neutrino-flavor conversion (FFC) plays an important role on NS kick. FFC is associated with one of flavor instabilities in collective neutrino oscillation [34], in which flavor correlation (or coherence) grows exponentially due to refractive effects of neutrino self-interactions (see reviews,

---

[*] hiroki.nagakura@nao.ac.jp
[†] sumi@numazu-ct.ac.jp

e.g., [35–39]). Recent studies suggest that the flavor instability occurs for wide mass range of progenitors by various mechanisms [40,41] and the stellar rotation would facilitate the occurrence of FFC [42]. Since the flavor conversion can occur in a much shorter timescale than the dynamical timescale of the system, neutrino radiation field is instantaneously changed by flavor conversions, once the instability switches on. In this paper, we show that occurrences of FFC in asymmetric neutrino radiation field can further enhance the asymmetry, which potentially generates high velocities of NS natal kick.

This paper is organized as follows. In Sec. II, we first describe our basic picture of how FFC can give a linear momentum to NS. We then strengthen our arguments by performing Boltzmann neutrino transport simulations under CCSN fluid profiles, in which we incorporate effects of FFCs by a phenomenological prescription. The numerical methods and models are summarized in Sec. III and the results are summarized in Sec. IV. We conclude our work in Sec. V.

## II. FFC-DRIVEN NEUTRON STAR KICK

Assuming that muon-type ($\nu_\mu$) and tau-type neutrinos ($\nu_\tau$), which are collectively denoted as $\nu_x$, and their antipartners ($\bar{\nu}_x$) are identical, the onset of FFC is dictated by the disparity of angular distributions of electron-type neutrinos ($\nu_e$) and their antipartners ($\bar{\nu}_e$) (but see also [43] when we take into account differences between $\nu_x$ and $\bar{\nu}_x$). More specifically, electron-type lepton number ($\nu_e$-$\bar{\nu}_e$ or ELN) angular crossings marks the onset of the flavor instability [44]. It has been suggested that the crossing tends to occur in regions where the number densities of $\nu_e$ and $\bar{\nu}_e$ ($n_{\nu_e}$ and $n_{\bar{\nu}_e}$) are close to each other [45,46]. Following the convention in this field, we use $\alpha$ to measure the asymmetry of number densities of $\nu_e$ ($n_{\nu_e}$) and $\bar{\nu}_e$ ($n_{\bar{\nu}_e}$), which is defined as

$$\alpha \equiv \frac{n_{\bar{\nu}_e}}{n_{\nu_e}}. \tag{1}$$

It should be mentioned that FFCs do not occur inside proto-neutron star (PNS) ($\rho \gtrsim 10^{14}$ g/cm$^3$, where $\rho$ denotes the baryon mass density), since $n_{\nu_e}$ is much larger than $n_{\bar{\nu}_e}$, i.e., $\alpha \ll 1$ due to strong degeneracy of $\nu_e$.[1] In the PNS envelope ($10^{11}$ g/cm$^3 \lesssim \rho \lesssim 10^{14}$ g/cm$^3$), on the other hand, the chemical potential of $\nu_e$ decreases and matter temperature increases with radius, resulting in a rapid decrease of $\nu_e$ degeneracy. Spherically symmetric CCSN models have showed, however, that the chemical potential of $\nu_e$ is still high enough to suppress ELN angular crossings, implying that the neutrino distributions are stable to FFC [47,48]. However, the situation can be qualitatively changed in multidimensional models. For instances, PNS convections facilitate deleptonization of CCSN core [49], that results in decreasing electron-fraction ($Y_e$), and consequently the degeneracy of $\nu_e$ is lower than spherically symmetric models, and it could be even negative. This implies the region with $\alpha \sim 1$ appears in the convective layer. Since the anisotropy of $\bar{\nu}_e$ in momentum space is relatively higher than $\nu_e$, ELN angular crossings emerge in these regions [50,51].

Another representative FFC in multidimensional CCSN models is triggered by large-scale coherent asymmetric neutrino emission. The asymmetric neutrino emission is accompanied by a radiation-hydrodynamical instability, namely lepton-emission self-sustained asymmetry (LESA [52–54]) or coherent asymmetric $Y_e$ distributions associated with PNS kick [24]. Due to the anticorrelation of asymmetric neutrino emission between $\nu_e$ and $\bar{\nu}_e$, $\alpha$ becomes close to unity in the region where $Y_e$ is low and $\bar{\nu}_e$ ($\nu_e$) is stronger (weaker), generating ELN angular crossings [41,46]. As we show below, the NS kick can be accompanied by this type of FFC associated with asymmetric neutrino emission.

One may wonder why FFC can impart a linear momentum to NS. In fact, no linear momentum are generated only by FFCs, because the flavor conversion changes flavor states but the flavor-integrated energy and momentum are conserved. The key player is neutrino-matter interactions such as neutrino emission, absorption, and scatterings. Since they depend on neutrino flavors, the exchange of momentum between neutrinos and matter is affected by FFCs.

Our NS kick scenario was inspired by results from previous studies. It has been shown in numerical simulations that FFCs can enhance neutrino cooling if they occur in optically thick or semitransparent regions. This trend has been observed rather commonly regardless of different approaches, e.g., global neutrino-radiation-hydrodynamic simulations of CCSNe and binary neutron star mergers (BNSMs) with phenomenological approaches of FFC [55–59] and direct quantum kinetic simulations [60,61]. The physical mechanism can be understood as follows. In general, electron-type neutrinos are more abundant than heavy-leptonic ones, implying that FFC works to reduce the number of electron-type neutrinos. On the other hand, heavy-leptonic neutrinos have lower opacities than electron-type ones due to the lack of charged-current reactions,[2] implying that heavy-leptonic neutrinos can easily escape from the region. This indicates that the

---

[1] We note that FFC may occur in the high density region in the late postbounce (or PNS cooling) phase, since the $\nu_e$ degeneracy becomes mild due to deleptonization.

[2] We note that on-shell muons may appear in the envelop of PNS [62–64]. However, the muon number density is much lower than that of electrons, indicating that the trend is qualitatively similar in this case.

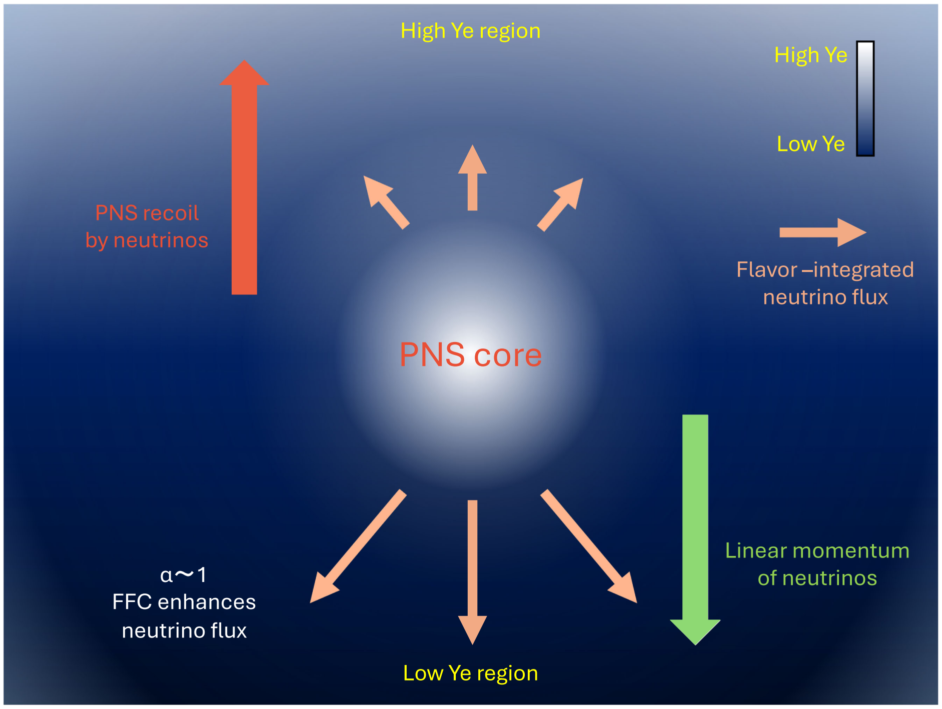

FIG. 1. Schematic picture of FFC-driven NS kick. Background color represents $Y_e$; white and black regions correspond to high- and low $Y_e$ regions, respectively. FFC occurs in low $Y_e$ region, which leads to high flavor-integrated neutrino fluxes (see the text for more details). This generates a linear momentum of neutrinos in the low $Y_e$ direction (green arrow), and consequently the NS obtains the same amount of linear momentum in the opposite direction to the neutrino linear momentum (red arrow).

increase of heavy-leptonic neutrinos by FFCs results in increasing neutrino flux. Due to the large neutrino flux of heavy-leptonic neutrinos, FFCs keep converting electron-type neutrinos to heavy-leptonic ones, while electron-type neutrinos are produced by charged-current reactions. As a result, neutrinos can extract energies from matter more efficiently by FFCs. This leads to the acceleration of neutrino cooling. We note that neutrinos can carry not only the energy but also momentum, indicating that momentum loss by neutrinos are also enhanced by FFC. This results in generating a linear momentum.

Let us summarize the FFC-driven NS kick scenario (see also Fig. 1). In PNS envelope, large-scale asymmetric matter distributions are created for some reason (e.g., LESA), and $Y_e$ in some regions can be low enough to generate ELN angular crossings, leading to occurrences of FFCs. Because electron-type neutrinos are more populated than other species, the flavor conversion increases the number density of heavy-leptonic one, while heavy-leptonic neutrinos are more transparent than electron-type neutrinos, leading to the increase of neutrino flux. The flux reduces the number density of heavy-leptonic neutrinos, which sustains the flavor conversion from electron-type to heavy-leptonic neutrinos, while electron-type neutrinos can be efficiently produced by charged-current reactions. This implies that neutrinos and matter in the region share the momentum each other more efficiently than in other regions, breaking the global momentum balance in the system, which gives a linear momentum to NS.

This mechanism suggests that the direction of NS kick should be in the direction with higher-$Y_e$ environment, implying that this process generate a correlation between ejecta composition and NS kick direction (see also [65]). The x-ray observations for young SNRs, which have the ability to measure spatial distributions of heavy elements (see, e.g., [66]), would be very useful to place a constraint of the mechanism. We also note that more detailed information may be given near future by XRISM mission [67].

To strengthen our proposed scenario, we demonstrate in the following sections that FFCs can induce linear momentum of neutrinos by performing axisymmetric Boltzmann neutrino transport simulations. It should be noted that these simulations are meant as a proof-of-principle, and more detailed studies are needed to assess whether the FFC-driven NS kick mechanism can be responsible for observed velocities of NS proper motions. Nevertheless, we demonstrate that the FFC has the ability to change a linear momentum of neutrinos by $\sim$ a few $\times 10^{40}$ g cm/s. This represents a possibility that the FFC-driven mechanism is a new channel to contribute NS natal kick.

## III. NUMERICAL METHOD AND MODEL

In this section, we describe some essential information of our numerical method and model in our neutrino transport simulations. In Sec. III A, we first describe the background fluid profile. In Sec. III B, we summarize our neutrino transport code and also describe an approximate neutrino-mixing scheme to include effects of FFCs into classical neutrino transport.

### A. Fluid distribution

In this study, we refer a fluid profile from a spherically symmetric CCSN model, which was developed by a numerical code for a neutrino-radiation hydrodynamics with full Boltzmann neutrino transport [68]. In the simulation, the neutrino radiation field is determined by solving the Boltzmann equation. We adopt the fluid profile at 300 ms after the core bounce obtained by following the time evolution from the Fe core of the $15M_{\odot}$ star by [69]. The equation of state by the variational method [70] was adopted in the simulation and the same equation of state is used in the current study.

As mentioned in Sec. II, spherically symmetric CCSN models are unlikely to generate ELN angular crossings in the post shock region, and we confirmed that there are no ELN angular crossings in our neutrino data. This is mainly due to the high $Y_e$ distributions compared to multidimensional models (see [49]), since higher $Y_e$ leads to stronger degeneracy of $\nu_e$. $Y_e$ needs to be, hence, lower in order to generate ELN angular crossings (or FFCs). Another important condition for the FFC-driven NS kick scenario is that $Y_e$ distributions need to be globally asymmetric; more specifically, it should have a dipole asymmetry. Based on the above considerations, we assume that $Y_e$ has a dipole deformation, which is given as

$$Y_e(r,\theta) = Y_e^{1D}(r)(1+\epsilon\cos\theta), \tag{2}$$

where $\theta$ is the polar angle measured from the $z$-axis, and $Y_e^{1D}$ denotes the $Y_e$ profile in a spherically symmetric CCSN model. In the expression $\epsilon$ represents a deformation parameter, and we set $\epsilon = 0.15$. As we shall show in Sec. IV A, ELN angular crossings appear in the southern hemisphere, i.e., lower-$Y_e$ region in the classical neutrino transport simulation (baseline model; see below for more details). We note that the matter distributions are frozen during the neutrino transport simulations.

Let us remark a few caveats about fluid background. First, one has to keep in mind that the deformed $Y_e$ profile given by Eq. (2) is not realistic but rather a toy model. The artificial change of fluid distributions would lead to unphysical equilibrium state between neutrino and matter. In fact, high- (low-)$Y_e$ region has stronger $\nu_e$ ($\bar{\nu}_e$) emission, making neutrino distributions approach towards a different chemical equilibrium state from the original one. More self-consistent treatment of neutrino-radiation fields is necessary for more quantitative arguments. We defer such simulations to future work.

As the other important remark, the asymmetric degree of $Y_e$ in the present study ($\epsilon = 0.15$) is high compared to more realistic CCSN simulations. Again this setting is meant to construct a model to test our hypothesis. We note that the required asymmetry in $Y_e$ distribution for occurrences of FFC (or ELN angular crossings) strongly depends on the angle-averaged $Y_e$. In the present study, we adopt a spherically symmetric CCSN model, which has a systematically high $Y_e$ than that in multidimensional CCSN models due to suppression of PNS convection [49]. In fact, $\epsilon \lesssim 0.1$ is large enough for occurrences of FFCs in more realistic multidimensional models [41,46]. In the present study, we need to keep in mind these caveats to interpret our results.

We show in Fig. 2 the fluid profile employed in this study. As in the original spherically symmetric CCSN model, the distributions of density and temperature remain spherical. The outer radius of PNS envelope, which is defined at the density of $10^{11}$ g cm$^{-3}$, is ~40 km. At this time snapshot, the shock wave is located at ~90 km, where a large entropy jump is remarkable. Note that the distribution of entropy is not spherical due to the deformed distribution of $Y_e$. The $Y_e$ is higher on the north side than at the equator and lower on the south side due to the given deformation [see Eq. (2)]. This deformed distribution in $Y_e$ leads to the different neutrino distributions for $\nu_e$ and $\bar{\nu}_e$ accompanied by their anticorrelated asymmetric emission as we examine in the following.

### B. Classical neutrino transfer with FFC

The neutrino radiation field is determined by utilizing the numerical code to directly solve the Boltzmann equation [71]. This neutrino transport code has been used to model neutrino radiation field in static fluid backgrounds (see, e.g., [72,73]). It should be mentioned that we employ the Boltzmann transport code rather than the radiation-hydrodynamic one which has been used to develop multidimensional CCSN models [24,68,74–76]. As we shall describe in Sec. III B, the Boltzmann transport module needs to be extended so as to incorporate effects of FFCs in the present study; for instances, the number of neutrino species is increased from three to four, and a new module for neutrino-mixing also needs to be incorporated. These extensions are complicated for radiation-hydrodynamic code, because there are many other modules intertwined to the transport one. On the other hand, the code structure in [71] is simpler than the radiation-hydrodynamic one; hence, we employ the latter code in the present study. We note that the purpose of the simulations is to provide evidence that FFC can change a linear momentum in neutrino radiation field along with the scenario described in Sec. II, indicating that transport simulations in static fluid background satisfy the purpose of the present study.

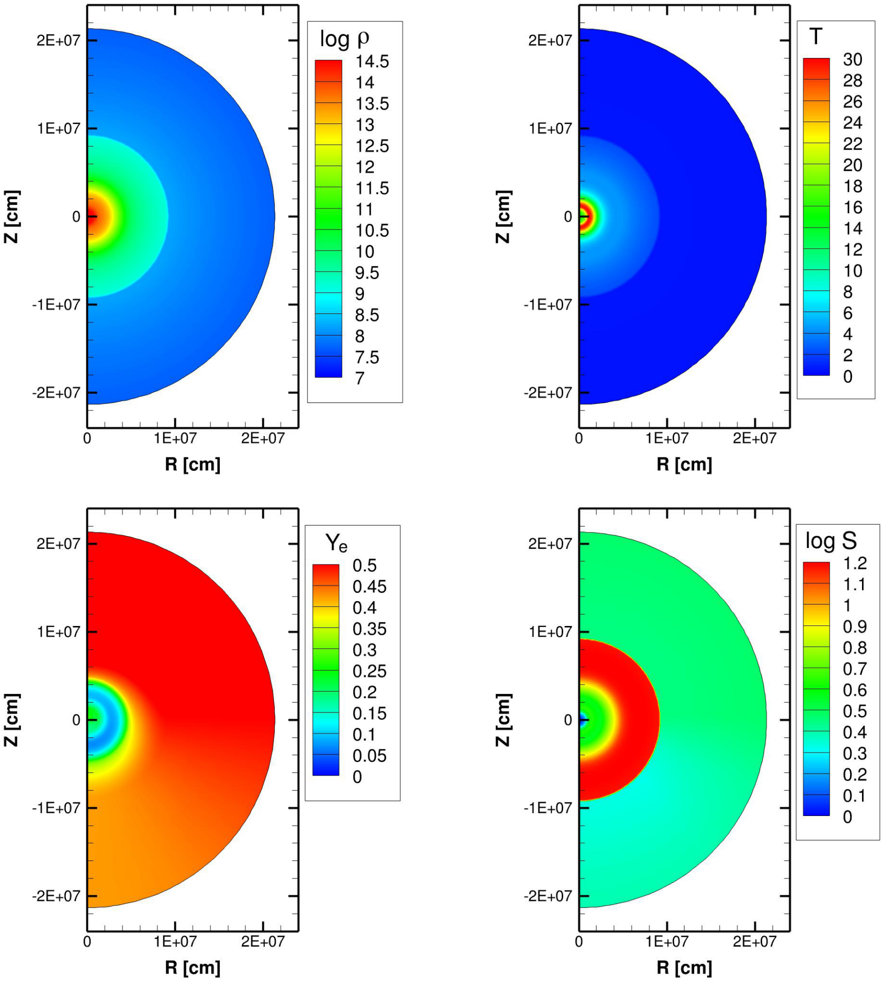

FIG. 2. Profiles of matter distributions employed in this study. Upper left, upper-right, lower-left, and lower-right panels show density ($\mathrm{g\,cm^{-3}}$), temperature (MeV), $Y_e$, and entropy per baryon ($k_B$), respectively. We note that density and temperature profiles are assumed to be in spherically symmetric, whereas $Y_e$ is deformed. This leads to a dipole deformation in entropy distribution. See text for more details.

Before describing the numerical setup, we make a few remarks about differences between the two codes. In our radiation-hydro code, we use a two-energy-grid technique [77], which was developed so as to to take into account fluid-velocity dependence in neutrino transport. On the other hand, such a technique is not used in [71], and we do not distinguish laboratory- and fluid-rest frames. It should also be mentioned that some updates of neutrino-matter interactions have been made in neutrino-radiation-hydro code; electron(positron)-scatterings, electron-capture by heavy nuclei, and weak interactions of light nuclei (see [78] for more details). For the sake of completeness, we checked the discrepancy in the results between two codes under spherically symmetric model, and found that $\nu_e$ and $\bar{\nu}_e$ fluxes in [71] are higher and lower, respectively, than those obtained in [74].

Although these discrepancies between the two codes prevent us from ascertaining quantitative impacts of FFC on NS kick, the transport code in [71] still has the ability to capture essential features for the FFC-induced NS kick scenario. In fact, our simulations successfully demonstrate that FFC increases energy fluxes of heavy-leptonic neutrinos, which corresponds to the most important ingredient in the mechanism.

Boltzmann equations are solved by the $S_n$ method. Under spatial axisymmetric condition, we determine the time evolution of the neutrino distributions as functions of radius ($r$), zenith angle ($\theta$), two angles ($\theta_\nu$ and $\phi_\nu$), and energy ($\varepsilon_\nu$) in momentum space. The radial and polar angle coordinates cover the range of 0–210 km and $0 \sim \pi$ by 256 and 128 grids, respectively. The neutrino energy is divided into 14 bins. The neutrino angle distributions, $\theta_\nu$ and $\phi_\nu$, are described by 10 and 6 bins, respectively.

We use the equation of state by the variational method with the mixture of nuclei under the nuclear statistical equilibrium [70] to obtain the thermodynamical properties and composition of hot and dense matter. The basic set of weak interaction (emission, absorption, pair production, and annihilation) is implemented in the collision term of the Boltzmann equation with angle- and energy-dependent expressions [71].

Given a static fluid background (Sec. III A), we follow the time evolution of neutrino distributions until the radiation field settles into a steady state. In this study, we run two simulations; baseline model and FFC model. The baseline model correspond to a purely classical transport case. In FFC model, we incorporate effects of FFCs on classical neutrino transport (see below).

To incorporate effects of flavor conversions, two updates in our Boltzmann solver are required. First, $\nu_x$ and $\bar{\nu}_x$ should be treated independently, since flavor conversions differentiate their distributions. Since our original Boltzmann solver has treated $\nu_x$ and $\bar{\nu}_x$ collectively (i.e., 3 species neutrino transfer), we updated the Boltzmann code to handle four species, ($\nu_e$, $\bar{\nu}_e$, $\nu_x$, $\bar{\nu}_x$).

The other necessary update is neutrino-mixing scheme. At each time step, we check if neutrino distributions have ELN-XLN (XLN denotes heavy-leptonic neutrino number) angular crossings at each spatial mesh. If they are detected, we shuffle neutrinos instantaneously as the following manner. The neutrino mixing is treated by introducing survival probability of $\nu_e$ ($p$) and $\bar{\nu}_e$ ($\bar{p}$) as

$$f_{\nu_e} = p f^0_{\nu_e} + (1-p) f^0_{\nu_x}, \tag{3}$$

$$f_{\bar{\nu}_e} = \bar{p} f^0_{\bar{\nu}_e} + (1-\bar{p}) f^0_{\bar{\nu}_x}, \tag{4}$$

for electron-type (anti)neutrinos and

$$f_{\nu_x} = \frac{1}{2}(1-p) f^0_{\nu_e} + \frac{1}{2}(1+p) f^0_{\nu_x}, \tag{5}$$

$$f_{\bar{\nu}_x} = \frac{1}{2}(1-\bar{p}) f^0_{\bar{\nu}_e} + \frac{1}{2}(1+\bar{p}) f^0_{\bar{\nu}_x}, \tag{6}$$

for $\mu$ and $\tau$-types (anti)neutrinos [79]. In the expression, $f^0$ denotes the distribution function of neutrinos before the mixing. Just for simplicity, we set $p = \bar{p} = \frac{1}{3}$ for all energies and angles, corresponding to flavor equipartition, in this study.

Let us make a few remarks about our neutrino mixing scheme. First, as pointed out by [80], the instantaneous mixing prescription suffers from a self-consistency issue. This issue can be resolved by more appropriate prescriptions such as miscidynamics [81] and the Bhatnagar-Gross-Krook (BGK) subgrid model [82]. It should be noted, however, that a recent study in [83] showed that classical neutrino transport with an instantaneous mixing scheme agreed reasonably well with results of quantum kinetic one. This would be attributed to the fact that FFCs occur in optically thick or semitransparent regions where neutrino self-interactions dominate over neutrino-matter interactions. Since we have in mind a scenario that FFC occurs in these regions, the instantaneous mixing prescription would be a reasonable approximation.

One may also speculate that shallow ELN angular crossings, which have been observed in multidimensional CCSN models [41,46], do not have abilities to lead flavor equipartition. According to detailed studies of asymptotic states of FFC [84,85], however, the shallow and narrow ELN angular crossings can lead to large flavor conversions and even flavor equipartition if $\nu_e$ and $\bar{\nu}_e$ number densities are nearly equal to each other [86]. In fact, we observed flavor equipartitions in CCSN models with quantum kinetic neutrino transport [60,61,87]. It should be noted, however, that the flavor equipartition corresponds to an extreme case and the actual flavor conversion may be less vigorous, indicating that the present study may overestimate the impact of FFC on NS kick. This exhibits that a higher fidelity scheme in the determination of asymptotic states of FFC (see, e.g., [85,88,89]) is necessary for a more quantitative discussion, but such an improvement is beyond the scope of this paper.

## IV. NUMERICAL RESULTS

### A. Baseline model (no flavor conversions)

Let us first highlight some important features of neutrino radiation field in baseline model, that is helpful to understand the result of FFC model. In Fig. 3, we display neutrino number densities for $\nu_e$, $\bar{\nu}_e$, and $\nu_x$. The distribution of $\nu_e$ is almost spherical but shifted to the north side due to the higher $Y_e$. Contrary to $\nu_e$, the distribution of $\bar{\nu}_e$ is shifted to the south side due to the lower $Y_e$. Hence, there is north-south antisymmetry between $\nu_e$ and $\bar{\nu}_e$ radiation fields. The distribution of $\nu_x$ is spherical at the center, reflecting the spherical distribution of density and temperature. This is because $\nu_x$ is thermally produced by pair-processes, and these processes are less sensitive to $Y_e$.

It would also be interesting to quantify the asymmetry of neutrino energy fluxes for different neutrino species at the outer boundary of computational domain ($r = 210$ km), which is shown in Fig. 4. The fluxes along the radial coordinate clearly exhibit that there are north-south asymmetries for $\nu_e$ and $\bar{\nu}_e$, in which the fluxes are larger in the north direction for the former and in the south direction for the latter, respectively. On the other hand, the energy flux of $\nu_x$ is much less angular dependent than $\nu_e$ and $\bar{\nu}_e$. These trends are consistent with the spatial distributions of neutrino number densities as shown in Fig. 3.

There are two important remarks here. First, the $\nu_e$ energy flux is remarkably higher than $\bar{\nu}_e$ in baseline model. This is partially due to the discrepancy between the two Boltzmann codes (see Sec. III A). It should also be mentioned that we adopt the angular averaged $Y_e$ [or $Y_e^{1D}$ in Eq. (2)] from a result of spherically symmetric CCSN model. As mentioned already, $Y_e$ tends to be higher around PNS envelope in spherically symmetric model due to lack

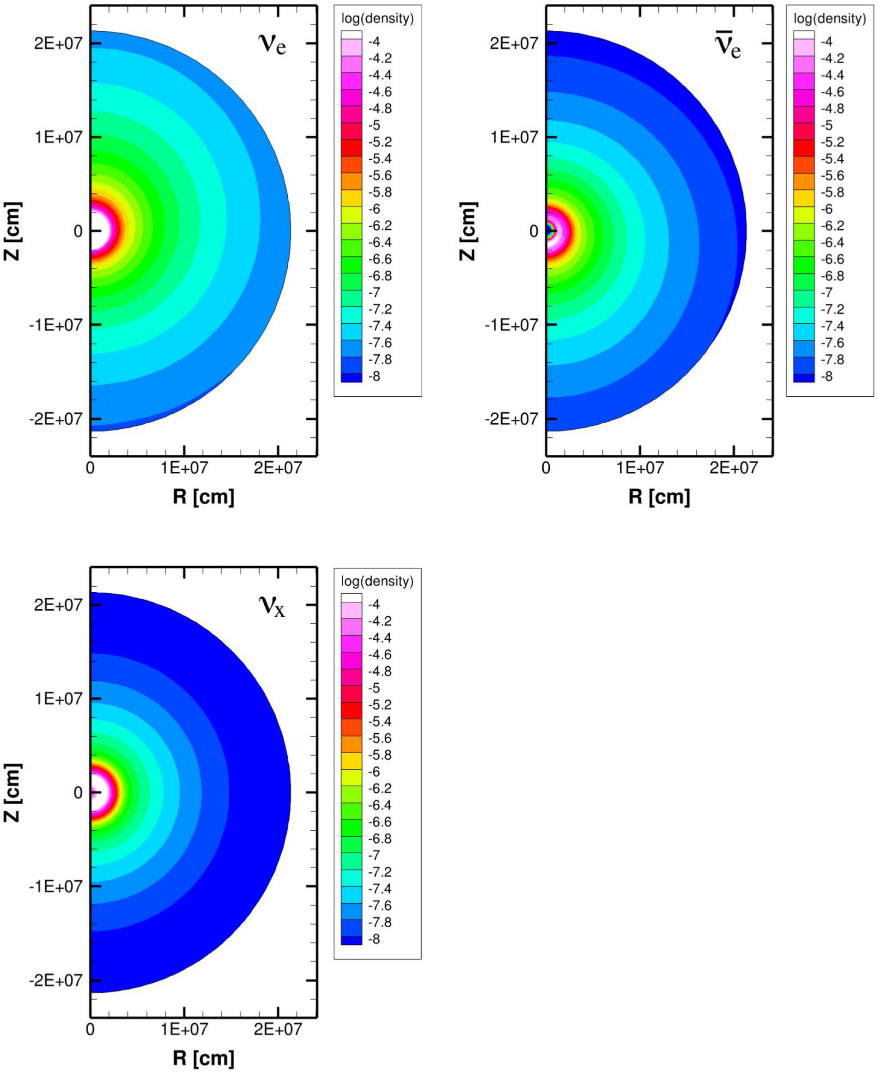

FIG. 3. Neutrino number densities obtained in baseline model are shown on the meridian slice by color contour map. The number densities in units of fm$^{-3}$ for $\nu_e$, $\bar{\nu}_e$, and $\nu_\mu$ are shown in upper-left, upper-right, and lower-left panels, respectively.

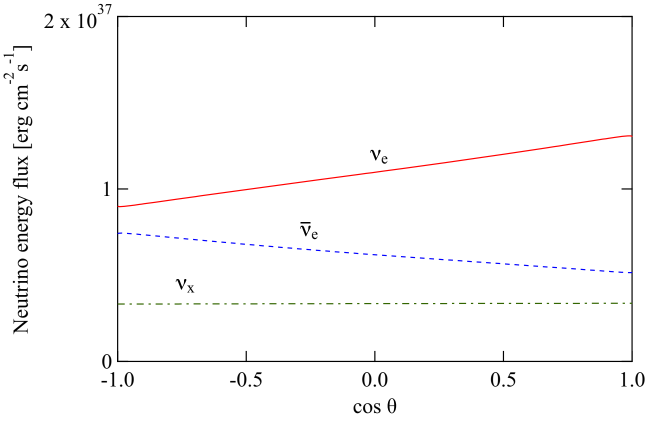

FIG. 4. Radial component of energy fluxes for each species of neutrinos at the outer boundary (210 km) for baseline model. Sold, dashed, and dot-dashed lines denote the energy flux of $\nu_e$, $\bar{\nu}_e$, and $\nu_\mu$, respectively.

of PNS convection [49]. The disparity between $\nu_e$ and $\bar{\nu}_e$ should be, hence, relaxed in more self-consistent multidimensional models. Second, the energy flux of $\nu_x$ is the lowest, but it does not mean that $\nu_x$ is subdominant to carry energies. Importantly, the $\nu_x$ represents a single species of heavy-leptonic neutrinos, indicating that their total fluxes is four times higher than the value displayed in Fig. 4. This also exhibits that the small asymmetry of $\nu_x$ can contribute the NS kick (see also [24]).

Figure 5 displays a 2D color map of $\alpha$ [ratio of the densities of $\bar{\nu}_e$ and $\nu_e$; see Eq. (1)] for baseline model. We find that a region with $\alpha \sim 1$ appears in the southern hemisphere. This offers a preferable condition for occurrences of FFC, which is portrayed in Fig. 6. In the figure, we highlight regions having ELN angular crossings by a green color, where the ELN angular distribution is defined as

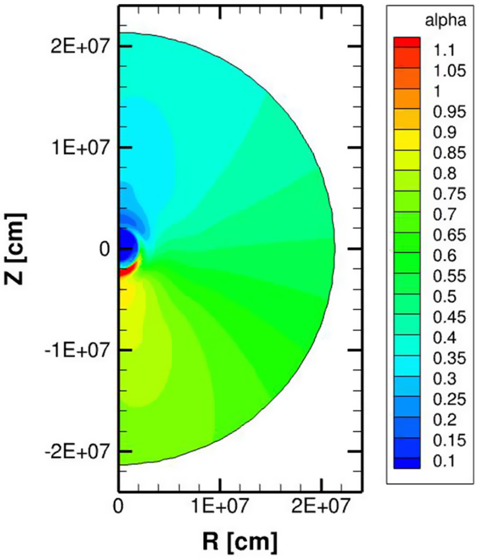

FIG. 5. Ratio of the number density of $\bar{\nu}_e$ to the number density of $\nu_e$ for baseline model is shown on the meridian slice by color map.

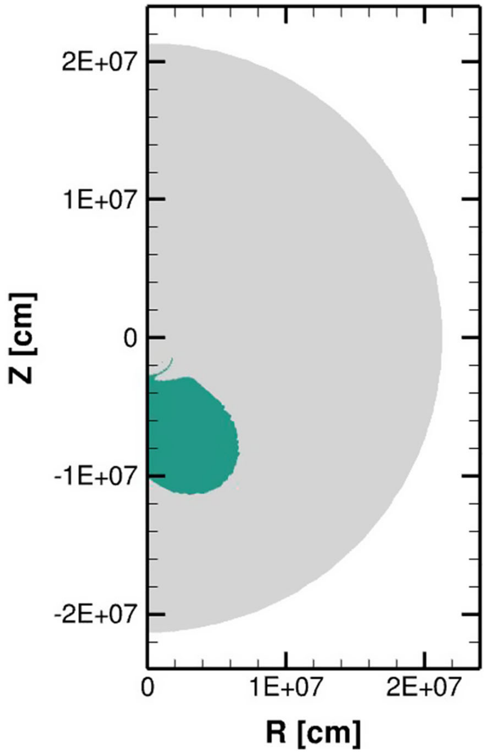

FIG. 6. 2D color map highlighting the region of the ELN angular crossing in baseline model.

$$G_{v_{\nu_e}} = \sqrt{2}\frac{G_F}{\hbar c}\int_0^\infty \frac{\varepsilon_\nu^2 d\varepsilon_\nu}{(hc)^3}\left[f_{\nu_e}(p_\nu) - f_{\bar{\nu}_e}(p_\nu)\right]. \tag{7}$$

In the expression, $G_F$, $\hbar$, and $c$ denote Fermi constant, reduced Planck constant, and the speed of light, respectively. We note that XLN is always zero in the baseline model, implying that the occurrences of FFC can be assessed only by ELN angular distributions. The occurrence of ELN angular crossing corresponds to the case that the sign of $G_{v_{\nu_e}}$ changes in the angular distribution. We find that ELN angular crossings occur in the region with $\alpha \sim 1$ (southern hemisphere), which corresponds to lower $Y_e$ region where $\bar{\nu}_e$ ($\nu_e$) emission is also stronger (weaker). This implies that FFC must occur in the region, which leads to a different steady radiation field in FFC model; the detail is discussed in the next subsection.

### B. FFC model

We show in Fig. 7 the neutrino number densities for $\nu_e$, $\bar{\nu}_e$, $\nu_x$, and $\bar{\nu}_x$. Let us remind the reader that $\nu_x$ and $\bar{\nu}_x$ are no longer identical in FFC model. We find that distributions of all species of neutrinos are very different from those in baseline model (see also Fig. 3). The $\nu_e$ distribution is shifted to the north side and has a rapid decline on the south side. This deficit arises from the conversion of $\nu_e$ to $\nu_x$ due to FFCs. The $\bar{\nu}_e$ distribution has a similar deformation in the opposite direction. It should be noted, however, that $\bar{\nu}_e$ in the southern region is somewhat diminished due to the conversion from $\bar{\nu}_e$ to $\bar{\nu}_x$, indicating that the asymmetry of $\bar{\nu}_e$ becomes mild compared to the baseline model. For $\nu_x$ and $\bar{\nu}_x$, they are enhanced in the southern region, which is due to flavor conversions from $\nu_e$ and $\bar{\nu}_e$, respectively.

In Fig. 8, we display the energy fluxes for all species of neutrinos, measured at the outer boundary ($r = 220$ km). This corresponds to the counterpart of Fig. 4 that displays the result of baseline model. It is worthy of note that $\nu_e$ and $\nu_x$ have nearly the same flux to each other at $\cos\theta = -1$ (or the south pole), while $\bar{\nu}_e$ and $\bar{\nu}_x$ also reach nearly flavor equipartition there. We note that the same trend has also been observed in quantum kinetic neutrino transport simulations [60,61], in which neutrinos and antineutrinos have different flavor equipartition states. This exhibits that the qualitative trend of nonlinear evolutions of FFCs is captured by our mixing scheme [see Eqs. (3)–(6)] with a condition of flavor equipartition.

As displayed in Figs. 7 and 8, it is noteworthy that the asymmetry of $\nu_x$ is higher than $\bar{\nu}_x$. This trend can be understood from the result of baseline model. As shown in Fig. 5, $\nu_e$ number density in the southern region is still higher than $\bar{\nu}_e$ except for the inner region of PNS envelop (20 km $\lesssim r \lesssim$ 25 km). Relevant to this trend, $\nu_e$ flux at the outer boundary is also higher than $\bar{\nu}_e$ in the southern region (see the region of $\cos\theta < 0$ in Fig. 4). In such an environment, neutrinos undergo more flavor conversions than antineutrinos [60,61]. It should be mentioned that this is not only due to FFC but also neutrino-matter interactions. In general, FFC is a pairwise conversion, indicating that the number of neutrinos and antineutrinos that experience flavor conversions should be the same. However, the collision term, in particular emission and absorption processes,

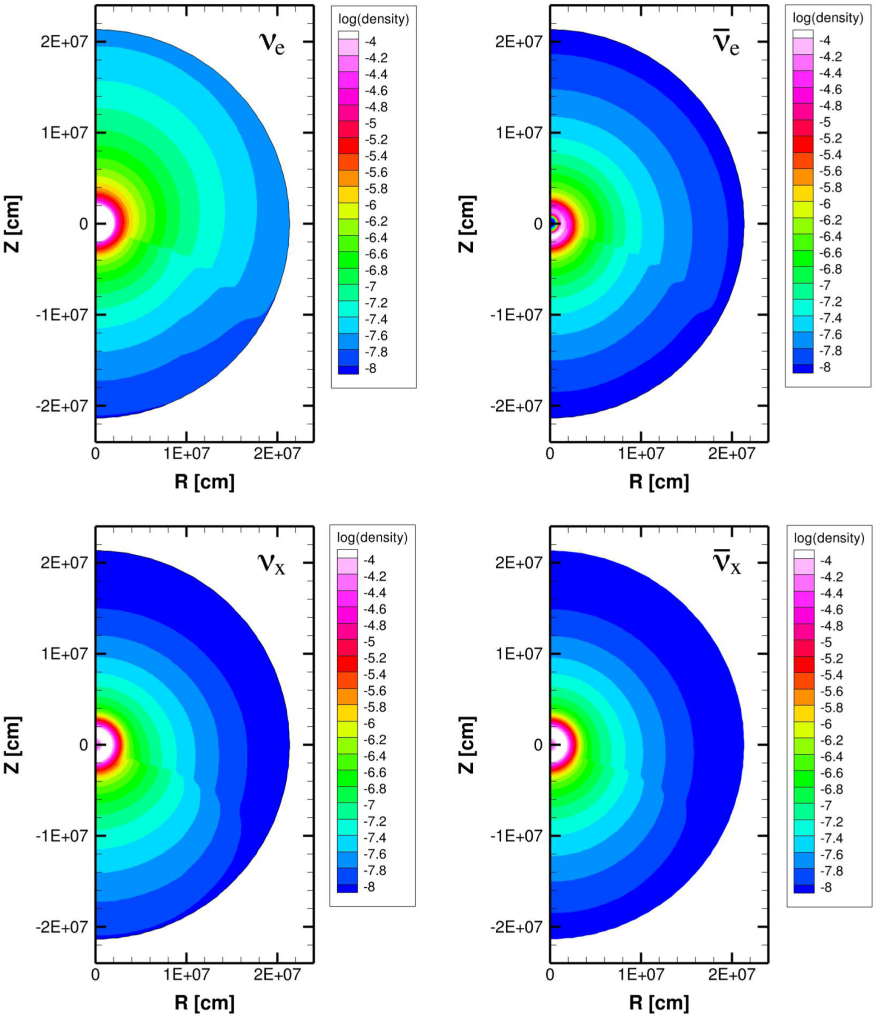

FIG. 7. Same as Fig. 3 but for FFC model. Since $\nu_x$ and $\bar{\nu}_x$ are no longer identical, they are displayed in different panels: $\nu_e$ (upper-left), $\nu_x$ (lower-left), $\bar{\nu}_e$ (upper-right), and $\bar{\nu}_x$ (lower-right).

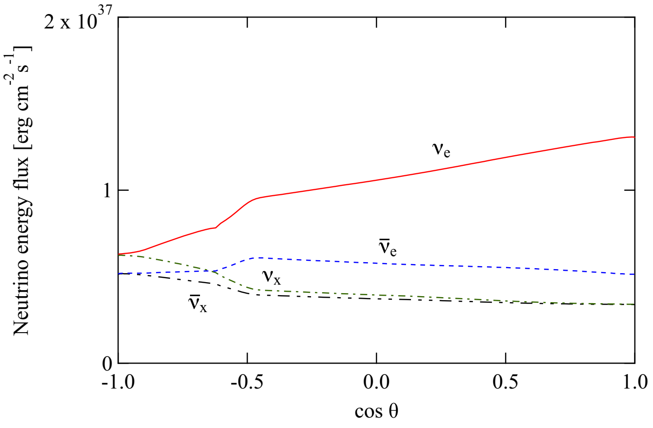

FIG. 8. Same as Fig. 4 but for FFC model. Solid (red), dashed (blue), dot-dashed (green), and dot-dot-dashed (black) lines denote the energy flux of $\nu_e$, $\bar{\nu}_e$, $\nu_x$, and $\bar{\nu}_x$, respectively.

can change the number of neutrinos and antineutrinos, which is responsible for the difference between $\nu_x$ and $\bar{\nu}_x$ in FFC model.[3] The dominance of $\nu_e$ indicates that the charged-current reaction of $\nu_e$ is stronger than $\bar{\nu}_e$. As a result, both the number density and flux of $\nu_x$ tend to be larger than those in $\bar{\nu}_x$.

However, there is a caveat to keep in mind that this trend ($n_{\nu_x} > n_{\bar{\nu}_x}$) may disappear in more realistic CCSN models. As already pointed out in Sec. IV A, the angular-averaged $Y_e$ profile in PNS envelop is higher in our model (because we adopt the $Y_e$ profile from a spherically symmetric CCSN simulation), that results in stronger $\nu_e$ emission in the entire direction. This would be an artifact and the trend is at least reduced in more realistic situations. Nevertheless,

---

[3] It should be noted that our approximate mixing scheme does not guarantee the pairwise conversion.

our numerical simulations lend confidence our claim that both number densities and fluxes for $\nu_x$ and $\bar{\nu}_x$ become higher in the southern region, enhancing a linear momentum in neutrino radiation field. Below, we quantify the linear momentum of neutrinos for both baseline and FFC models, and we show that the result is in line with our FFC-driven NS kick scenario as described in Sec. II.

### C. Linear momentum carried by neutrinos

We estimate linear momentum of neutrinos by following [27]. Assuming steady state of neutrino radiation field, the total momentum balance of neutrinos in the $z$-direction can be written as

$$\sum_i \frac{1}{r^2 \sin\theta} \partial_\alpha \left( r^2 \sin\theta T^{\alpha z}_{\nu_i} \right) = \sum_i G^z_{\nu_i}, \tag{8}$$

where $T^{\alpha z}_{\nu_i}$ and $G^z_{\nu_i}$ are the $z$-projection of the energy-momentum tensor of neutrinos and the momentum gain/loss by neutrino-matter interactions, respectively. In the expression, the index $i$ specifies the neutrino species: $\nu_i = \nu_e, \bar{\nu}_e, \nu_\mu, \bar{\nu}_\mu, \nu_\tau, \bar{\nu}_\tau$. The energy-momentum tensor of neutrinos can be computed as

$$T^{\alpha\beta}_{\nu_i} = \int \frac{d\varepsilon\, \varepsilon^2}{(2\pi)^3} \int d\Omega\, \varepsilon\, n^\alpha\, n^\beta\, f_{\nu_i}(\varepsilon, \Omega), \tag{9}$$

where $f_{\nu_i}$ is the distribution function of neutrino, and $n^\alpha$ is the unit vector specifying neutrino flight directions in four-dimensional spacetime. Note that the energy-momentum tensor depends on space, although we omit to show them in Eq. (9) just for simplicity.

The linear momentum carried by neutrinos per unit time at the surface of $r$ ($P^z_{\nu_i}$ which has a dimension of $gcm/s^2$) can be computed as

$$P^z_{\nu_i}(r) = 2\pi r^2 \int_0^\pi T^{rz}_{\nu_i}(r, \theta) \sin\theta d\theta, \tag{10}$$

where the $z$-projection of the radial component of the energy-momentum tensor, $T^{rz}_{\nu_i}$, is given by

$$T^{rz}_{\nu_i} = T^{rr}_{\nu_i} \cos\theta - T^{r\theta}_{\nu_i} \sin\theta. \tag{11}$$

We note that the flavor-integrated $P^z_{\nu_i}$ can also be evaluated from the volume integral of $G^z_{\nu_i}$ as [see Eq. (8)]

$$\sum_i P^z_{\nu_i}(r) = \sum_i 2\pi \int_0^r \int_0^\pi r^2 \sin\theta\, G^z_{\nu_i}(r', \theta)\, d\theta dr', \tag{12}$$

which represents the linear momentum transfer from matter to neutrinos. Because of the conservation of law of total energy and momentum in the system, the fluid needs to gain the linear momentum of the opposite sign of Eq. (12), representing the recoil by asymmetric neutrino emission. This leads to a NS natal kick.

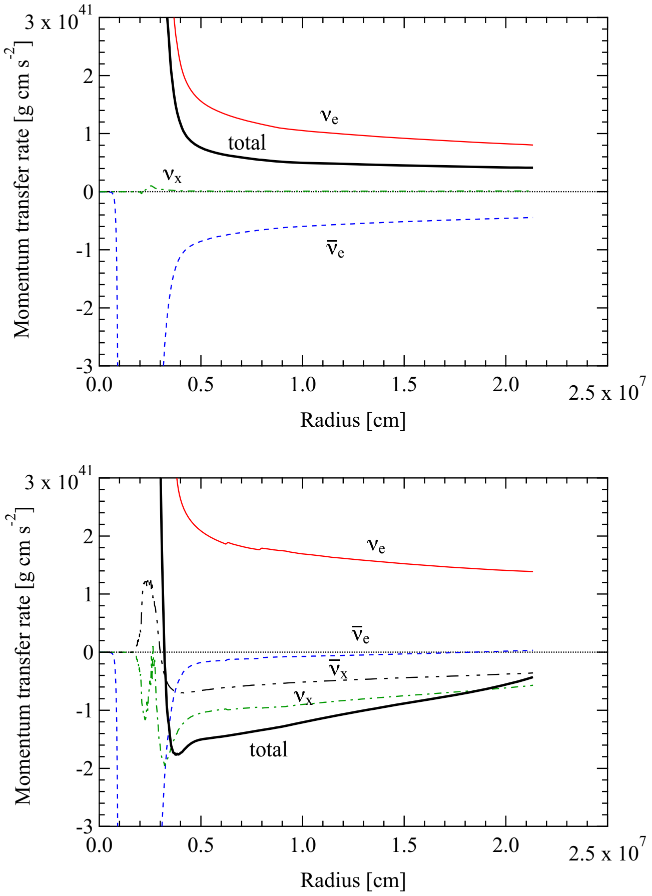

FIG. 9. Rates of momentum transfer in the $z$-direction are shown for baseline and FFC models as functions of radius in upper and lower panels, respectively. Solid (red), dashed (blue), dot-dashed (green), and dot-dot-dashed (black) lines denote the rate for $\nu_e$, $\bar{\nu}_e$, $\nu_x$, and $\bar{\nu}_x$, respectively. Thick lines denote the total rate.

In Fig. 9, we compare the species dependent $P^z_{\nu_i}$ as a function of radius for both baseline (upper-panel) and FFC (lower-panel) models. In baseline model (upper panel), $\nu_x$ is nearly spherical, and hence their linear momentum is negligible. On the other hand, $\nu_e$ has higher emission than $\bar{\nu}_e$, while the asymmetric degree is roughly the same to each other. As a result, the total linear momentum is in the direction of $\nu_e$, i.e., the northern direction (or high $Y_e$ hemisphere) in the baseline model. As shown in the lower panel, however, FFCs substantially change the linear momentum of neutrinos. Interestingly, the linear momentum carried by the sum of $\nu_e$ and $\bar{\nu}_e$ is in the northern direction, and the magnitude is even larger than the baseline model. This is attributed to the fact that the global asymmetries in $\nu_e$ ($\bar{\nu}_e$) emission are enhanced (reduced) by FFCs (see Sec. IV B). Nevertheless, the total flavor-integrated linear momentum is flipped and pointed in the southern direction (or low $Y_e$ hemisphere), indicating that the linear momentum carried by $\nu_x$ and $\bar{\nu}_x$ overwhelm $\nu_e$ and $\bar{\nu}_e$. This is exactly what we expected in our FFC-driven NS kick scenario (see Sec. II). The total neutrino emission is enhanced in the region where FFC occurs. We also find that the increase of $\nu_x$ asymmetry is remarkable, representing many $\nu_e$s in the southern direction undergo flavor conversions to $\nu_x$.

As shown in Fig. 9, the total linear momentum carried by neutrinos per unit time is $\sim 5 \times 10^{40}\ \mathrm{g\,cm/s^2}$ and $\sim -5 \times 10^{40}\ \mathrm{g\,cm/s^2}$ at the outer boundary for baseline and FFC models, respectively, which exhibits that FFCs change the linear momentum of neutrinos by $\sim 10^{41}\ \mathrm{g\,cm/s^2}$. One thing we do emphasize here is that this is a rough estimation and detailed inspections are necessary for more quantative arguments. In fact, the total linear momentum does not reach the asymptotic value at the outer boundary. The change of total momentum at the outer radii is mainly due to the coherent scattering by heavy nuclei, which corresponds to the dominant opacity source for neutrinos in preshock region. In the hemisphere of higher luminosity, neutrinos undergo those scattering more frequent than in the other hemisphere, leading to the decrease of total linear momentum. This potentially reduces the impact of FFCs on NS kick, suggesting that the feedback should be taken into account for more accurate estimation.

The lifetime of asymmetric neutrino emission depends on CCSN dynamics, but it would be typically a few hundred of milliseconds [24,46,52–54], suggesting that the impact of FFC in total linear momentum could be ∼ a few $\times 10^{40}\ \mathrm{g\,cm/s}$. This indicates FFC potentially has the ability to change the linear momentum of neutrinos by this order, i.e., generating ∼ a few $\times 0.1\%$ asymmetry with respect to the total neutrino emission. It should be emphasized, however, that the present study is meant as a proof-of-principle, and our model is too simple to draw robust conclusion whether the mechanism can account for the observed velocity distributions of NS proper motions. Nevertheless, this demonstration offers a possibility that globally asymmetric FFCs can induce NS natal kick.

## V. SUMMARY

In this paper, we propose a new channel to generate a neutron star (NS) natal kick during developments of CCSN explosions, upon which fast neutrino-flavor conversion (FFC), one of the quantum kinetic features of neutrinos, plays an important role. FFC tends to occur in the low-$Y_e$ environments, in which the $\nu_e$ degeneracy becomes mild and consequently ELN angular crossings can occur. The large-scale asymmetric $Y_e$ distributions have been observed in recent multidimensional CCSN models such as LESA [52–54] and a feedback mechanism between asymmetric neutrino emission and NS kick [24]. As shown in [41,46], FFC can occur in such asymmetric neutrino radiation fields, and we make a statement in this paper that the linear momentum of neutrinos are enhanced by FFCs in the hemisphere of low-$Y_e$ environment.

One thing we do notice here is that this scenario is inspired by previous studies, and it has been reached a consensus that the enhancement of neutrino cooling is one of the characteristic features of FFC. This is attributed to the fact that FFC can increase the number of heavy-leptonic neutrinos, while they are more optically thin than electron-type neutrinos due to the lack of charged-current reactions. This indicates that the opacity for flavor-integrated neutrinos are reduced by FFCs, leading to the enhancement of neutrino cooling. Since the neutrinos carry not only energy but also momentum, a linear momentum can also be generated (see Sec. II for more details of the FFC-driven NS kick mechanism).

We also perform axisymmetric neutrino transport simulations, which validates our proposed scenario. In our models, we deform the fluid background, in particular $Y_e$ distribution, as a dipole shape, which can generate linear momentum of neutrinos in z-direction. In the present study, we perform two simulations, one of which corresponds to a purely classical model (baseline model) and the other incorporates effects of FFC in a phenomenological way (FFC model). We show that FFC enhances a neutrino momentum in the direction of low-$Y_e$ environment and also provide physical processes how to generate the linear momentum. We also note that FFC-driven NS kick mechanism makes the NS to accelerate in the high-$Y_e$ direction, indicating that the asymmetric distributions of synthesized heavy elements in the ejecta would be correlated to the NS kick direction. This will be checked by future observations of SNR.

To compare these observations, we need more detailed study for FFC-driven NS kick scenario based on three-dimensional CCSN simulations by systematically changing progenitor models. It should also be mentioned that more accurate prescriptions for FFC are also necessary for quantitative arguments. In fact, we assume that flavor equipartition achieves for all places where ELN-XLN angular crossings appear. However, this treatment is obviously a crude treatment, and it should be improved in future studies. A new subgrid model, namely the BGK-model in [82], will help us to carry out global CCSN simulations with better FFC prescriptions; the results will be reported in our forthcoming papers.

## ACKNOWLEDGMENTS

This work is supported by the HPCI System Research Project (Projects No. 220173, No. 220047, No. 220223, No. 230033, No. 230204, and No. 230270), XC50 of CfCA at the National Astronomical Observatory of Japan (NAOJ), Yukawa-21 at Yukawa Institute for Theoretical Physics of Kyoto University, Research Center for Nuclear Physics, Osaka University, Information Technology Center, University of Tokyo, and the High Energy Accelerator

Research Organization (KEK). For providing high performance computing resources, Computing Research Center, KEK, and JLDG on SINET of NII are acknowledged. H. N. is supported by Grant-in-Aid for Scientific Research (23K03468). K. S. is supported by Grant-in-Aid for Scientific Research (19K03837, 20H01905, 24K00632). This work is supported by MEXT as "Program for Promoting Researches on the Supercomputer Fugaku" (Structure and Evolution of the Universe Unraveled by Fusion of Simulation and AI, JPMXP1020230406) and the Particle, Nuclear and Astro Physics Simulation Program (No. 2021-004, No. 2022-003, and No. 2023-003) of Institute of Particle and Nuclear Studies, High Energy Accelerator Research Organization (KEK).

[1] L. Wang and J. C. Wheeler, Spectropolarimetry of supernovae, Annu. Rev. Astron. Astrophys. **46**, 433 (2008).

[2] F. J. Abellán *et al.*, Very deep inside the SN 1987A core ejecta: Molecular structures seen in 3D, Astrophys. J. Lett. **842**, L24 (2017).

[3] G. Hobbs, D. R. Lorimer, A. G. Lyne, and M. Kramer, A statistical study of 233 pulsar proper motions, Mon. Not. R. Astron. Soc. **360**, 974 (2005).

[4] A. G. Lyne and D. R. Lorimer, High birth velocities of radio pulsars, Nature (London) **369**, 127 (1994).

[5] J. M. Cordes and David F. Chernoff, Neutron star population dynamics. II. Three-dimensional space velocities of young pulsars, Astrophys. J. **505**, 315 (1998).

[6] Z. Arzoumanian, D. F. Chernoff, and J. M. Cordes, The velocity distribution of isolated radio pulsars, Astrophys. J. **568**, 289 (2002).

[7] Claude-André Faucher-Giguère and Victoria M. Kaspi, Birth and evolution of isolated radio pulsars, Astrophys. J. **643**, 332 (2006).

[8] S. Chatterjee, W. H. T. Vlemmings, W. F. Brisken, T. J. W. Lazio, J. M. Cordes, W. M. Goss, S. E. Thorsett, E. B. Fomalont, A. G. Lyne, and M. Kramer, Getting its kicks: A VLBA parallax for the hyperfast pulsar B1508 + 55, Astrophys. J. **630**, L61 (2005).

[9] P. Frank Winkler and Robert Petre, Direct measurement of neutron star recoil in the oxygen-rich supernova remnant puppis A, Astrophys. J. **670**, 635 (2007).

[10] Tyler Holland-Ashford, Laura A. Lopez, Katie Auchettl, Tea Temim, and Enrico Ramirez-Ruiz, Comparing neutron star kicks to supernova remnant asymmetries, Astrophys. J. **844**, 84 (2017).

[11] Satoru Katsuda *et al.*, Intermediate-mass elements in young supernova remnants reveal neutron star kicks by asymmetric explosions, Astrophys. J. **856**, 18 (2018).

[12] Martin G. F. Mayer and Werner Becker, A kinematic study of central compact objects and their host supernova remnants, Astron. Astrophys. **651**, A40 (2021).

[13] Tyler Holland-Ashford, Patrick Slane, and Xi Long, Updated proper motion of the neutron star in the supernova remnant cassiopeia A, Astrophys. J. **962**, 82 (2024).

[14] Annop Wongwathanarat, Hans-Thomas Janka, and Ewald Müller, Hydrodynamical neutron star kicks in three dimensions, Astrophys. J. Lett. **725**, L106 (2010).

[15] J. Nordhaus, T. D. Brandt, A. Burrows, E. Livne, and C. D. Ott, Theoretical support for the hydrodynamic mechanism of pulsar kicks, Phys. Rev. D **82**, 103016 (2010).

[16] J. Nordhaus, T. D. Brandt, A. Burrows, and A. Almgren, The hydrodynamic origin of neutron star kicks, Mon. Not. R. Astron. Soc. **423**, 1805 (2012).

[17] A. Wongwathanarat, H.-T. Janka, and E. Müller, Three-dimensional neutrino-driven supernovae: Neutron star kicks, spins, and asymmetric ejection of nucleosynthesis products, Astron. Astrophys. **552**, A126 (2013).

[18] Hans-Thomas Janka, Neutron star kicks by the gravitational tug-boat mechanism in asymmetric supernova explosions: Progenitor and explosion dependence, Astrophys. J. **837**, 84 (2017).

[19] Adam Burrows, Tianshu Wang, David Vartanyan, and Matthew S. B. Coleman, A comprehensive theory for neutron star and black hole kicks and induced spins, Astrophys. J. **963**, 63 (2024).

[20] S. E. Woosley, The birth of neutron stars, in *The Origin and Evolution of Neutron Stars*, edited by D. J. Helfand and J. H. Huang (1987), Vol. 125, p. 255, https://ui.adsabs.harvard.edu/abs/1987IAUS..125..255W/abstract.

[21] G. S. Bisnovatyi-Kogan, Asymmetric neutrino emission and formation of rapidly moving pulsars, Astron. Astrophys. Trans. **3**, 287 (1993).

[22] Aristotle Socrates, Omer Blaes, Aimee Hungerford, and Chris L. Fryer, The neutrino bubble instability: A mechanism for generating pulsar kicks, Astrophys. J. **632**, 531 (2005).

[23] Christopher L. Fryer and Alexander Kusenko, Effects of neutrino-driven kicks on the supernova explosion mechanism, Astrophys. J. Suppl. Ser. **163**, 335 (2006).

[24] Hiroki Nagakura, Kohsuke Sumiyoshi, and Shoichi Yamada, Possible early linear acceleration of proto-neutron stars via asymmetric neutrino emission in core-collapse supernovae, Astrophys. J. Lett. **880**, L28 (2019).

[25] Matthew S. B. Coleman and Adam Burrows, Kicks and induced spins of neutron stars at birth, Mon. Not. R. Astron. Soc. **517**, 3938 (2022).

[26] C. L. Fryer, Neutron star kicks from asymmetric collapse, Astrophys. J. Lett. **601**, L175 (2004).

[27] Hiroki Nagakura, Kohsuke Sumiyoshi, and Shoichi Yamada, Three-dimensional Boltzmann-hydro code for core-collapse in massive stars. III. A new method for momentum feedback from neutrino to matter, Astrophys. J. **878**, 160 (2019).

[28] Hans-Thomas Janka, Annop Wongwathanarat, and Michael Kramer, Supernova fallback as origin of neutron star spins and spin-kick alignment, Astrophys. J. **926**, 9 (2022).

[29] Bernhard Müller, Fallback onto kicked neutron stars and its effect on spin-kick alignment, Mon. Not. R. Astron. Soc. **526**, 2880 (2023).

[30] E. R. Harrison and E. Tademaru, Acceleration of pulsars by asymmetric radiation, Astrophys. J. **201**, 447 (1975).

[31] Dong Lai, David F. Chernoff, and James M. Cordes, Pulsar jets: Implications for neutron star kicks and initial spins, Astrophys. J. **549**, 1111 (2001).

[32] J. Pétri, Impact of an off-centred dipole on neutron star binaries, Mon. Not. R. Astron. Soc. **488**, 4161 (2019).

[33] Andrei P. Igoshev, Martyna Chruslinska, Andris Dorozsmai, and Silvia Toonen, Combined analysis of neutron star natal kicks using proper motions and parallax measurements for radio pulsars and be x-ray binaries, Mon. Not. R. Astron. Soc. **508**, 3345 (2021).

[34] R. F. Sawyer, Speed-up of neutrino transformations in a supernova environment, Phys. Rev. D **72**, 045003 (2005).

[35] Irene Tamborra and Shashank Shalgar, New developments in flavor evolution of a dense neutrino gas, Annu. Rev. Nucl. Part. Sci. **71**, 165 (2021).

[36] Francesco Capozzi and Ninetta Saviano, Neutrino flavor conversions in high-density astrophysical and cosmological environments, Universe **8**, 94 (2022).

[37] Sherwood Richers and Manibrata Sen, Fast flavor transformations, in *Handbook of Nuclear Physics*, edited by I. Tanihata, H. Toki, and T. Kajino (Springer, Singapore, 2022).

[38] Maria Cristina Volpe, Neutrinos from dense: Flavor mechanisms, theoretical approaches, observations, new directions, arXiv:2301.11814.

[39] Tobias Fischer, Gang Guo, Karlheinz Langanke, Gabriel Martinez-Pinedo, Yong-Zhong Qian, and Meng-Ru Wu, Neutrinos and nucleosynthesis of elements, Prog. Part. Nucl. Phys. **137**, 104107 (2024).

[40] Sajad Abbar, Francesco Capozzi, Robert Glas, H. Thomas Janka, and Irene Tamborra, On the characteristics of fast neutrino flavor instabilities in three-dimensional core-collapse supernova models, Phys. Rev. D **103**, 063033 (2021).

[41] Hiroki Nagakura, Adam Burrows, Lucas Johns, and George M. Fuller, Where, when, and why: Occurrence of fast-pairwise collective neutrino oscillation in three-dimensional core-collapse supernova models, Phys. Rev. D **104**, 083025 (2021).

[42] Akira Harada and Hiroki Nagakura, Prospects of fast flavor neutrino conversion in rotating core-collapse supernovae, Astrophys. J. **924**, 109 (2022).

[43] Francesco Capozzi, Sajad Abbar, Robert Bollig, and H. Thomas Janka, Fast neutrino flavor conversions in one-dimensional core-collapse supernova models with and without muon creation, Phys. Rev. D **103**, 063013 (2021).

[44] Taiki Morinaga, Fast neutrino flavor instability and neutrino flavor lepton number crossings, Phys. Rev. D **105**, L101301 (2022).

[45] Sajad Abbar, Huaiyu Duan, Kohsuke Sumiyoshi, Tomoya Takiwaki, and Maria Cristina Volpe, On the occurrence of fast neutrino flavor conversions in multidimensional supernova models, Phys. Rev. D **100**, 043004 (2019).

[46] Hiroki Nagakura, Taiki Morinaga, Chinami Kato, and Shoichi Yamada, Fast-pairwise collective neutrino oscillations associated with asymmetric neutrino emissions in core-collapse supernovae, Astrophys. J. **886**, 139 (2019).

[47] Irene Tamborra, Lorenz Hüdepohl, Georg G. Raffelt, and Hans-Thomas Janka, Flavor-dependent neutrino angular distribution in core-collapse supernovae, Astrophys. J. **839**, 132 (2017).

[48] Taiki Morinaga, Hiroki Nagakura, Chinami Kato, and Shoichi Yamada, Fast neutrino-flavor conversion in the preshock region of core-collapse supernovae, Phys. Rev. Res. **2**, 012046 (2020).

[49] Hiroki Nagakura, Adam Burrows, David Radice, and David Vartanyan, A systematic study of proto-neutron star convection in three-dimensional core-collapse supernova simulations, Mon. Not. R. Astron. Soc. **492**, 5764 (2020).

[50] Robert Glas, H. Thomas Janka, Francesco Capozzi, Manibrata Sen, Basudeb Dasgupta, Alessandro Mirizzi, and Günter Sigl, Fast neutrino flavor instability in the neutron-star convection layer of three-dimensional supernova models, Phys. Rev. D **101**, 063001 (2020).

[51] Milad Delfan Azari, Shoichi Yamada, Taiki Morinaga, Hiroki Nagakura, Shun Furusawa, Akira Harada, Hirotada Okawa, Wakana Iwakami, and Kohsuke Sumiyoshi, Fast collective neutrino oscillations inside the neutrino sphere in core-collapse supernovae, Phys. Rev. D **101**, 023018 (2020).

[52] Irene Tamborra, Florian Hanke, Hans-Thomas Janka, Bernhard Müller, Georg G. Raffelt, and Andreas Marek, Self-sustained asymmetry of lepton-number emission: A new phenomenon during the supernova shock-accretion phase in three dimensions, Astrophys. J. **792**, 96 (2014).

[53] Robert Glas, H. Thomas Janka, Tobias Melson, Georg Stockinger, and Oliver Just, Effects of LESA in three-dimensional supernova simulations with multidimensional and ray-by-ray-plus neutrino transport, Astrophys. J. **881**, 36 (2019).

[54] Jade Powell and Bernhard Müller, Gravitational wave emission from 3D explosion models of core-collapse supernovae with low and normal explosion energies, Mon. Not. R. Astron. Soc. **487**, 1178 (2019).

[55] Xinyu Li and Daniel M. Siegel, Neutrino fast flavor conversions in neutron-star postmerger accretion disks, Phys. Rev. Lett. **126**, 251101 (2021).

[56] Oliver Just, Sajad Abbar, Meng-Ru Wu, Irene Tamborra, Hans-Thomas Janka, and Francesco Capozzi, Fast neutrino conversion in hydrodynamic simulations of neutrino-cooled accretion disks, Phys. Rev. D **105**, 083024 (2022).

[57] Rodrigo Fernández, Sherwood Richers, Nicole Mulyk, and Steven Fahlman, Fast flavor instability in hypermassive neutron star disk outflows, Phys. Rev. D **106**, 103003 (2022).

[58] Jakob Ehring, Sajad Abbar, Hans-Thomas Janka, Georg Raffelt, and Irene Tamborra, Fast neutrino flavor conversion in core-collapse supernovae: A parametric study in 1D models, Phys. Rev. D **107**, 103034 (2023).

[59] Jakob Ehring, Sajad Abbar, Hans-Thomas Janka, Georg Raffelt, and Irene Tamborra, Fast neutrino flavor conversions can help and hinder neutrino-driven explosions, Phys. Rev. Lett. **131**, 061401 (2023).

[60] Hiroki Nagakura, Roles of fast neutrino-flavor conversion on the neutrino-heating mechanism of core-collapse supernova, Phys. Rev. Lett. **130**, 211401 (2023).

[61] Hiroki Nagakura and Masamichi Zaizen, Basic characteristics of neutrino flavor conversions in the postshock regions

of core-collapse supernova, Phys. Rev. D **108**, 123003 (2023).

[62] R. Bollig, H. T. Janka, A. Lohs, G. Martínez-Pinedo, C. J. Horowitz, and T. Melson, Muon creation in supernova matter facilitates neutrino-driven explosions, Phys. Rev. Lett. **119**, 242702 (2017).

[63] Tobias Fischer, Gang Guo, Gabriel Martínez-Pinedo, Matthias Liebendörfer, and Anthony Mezzacappa, Muonization of supernova matter, Phys. Rev. D **102**, 123001 (2020).

[64] Gang Guo, Gabriel Martínez-Pinedo, A. Lohs, and Tobias Fischer, Charged-current muonic reactions in core-collapse supernovae, Phys. Rev. D **102**, 023037 (2020).

[65] Shin-ichiro Fujimoto and Hiroki Nagakura, Explosive nucleosynthesis with fast neutrino-flavour conversion in core-collapse supernovae, Mon. Not. R. Astron. Soc. **519**, 2623 (2023).

[66] Tyler Holland-Ashford, Laura A. Lopez, and Katie Auchettl, Asymmetries of heavy elements in the young supernova remnant cassiopeia A, Astrophys. J. **889**, 144 (2020).

[67] XRISM Science Team, Science with the x-ray imaging and spectroscopy mission (XRISM), arXiv:2003.04962.

[68] H. Nagakura, W. Iwakami, S. Furusawa, H. Okawa, A. Harada, K. Sumiyoshi, S. Yamada, H. Matsufuru, and A. Imakura, Simulations of core-collapse supernovae in spatial axisymmetry with full Boltzmann neutrino transport, Astrophys. J. **854**, 136 (2018).

[69] S. E. Woosley, A. Heger, and T. A. Weaver, The evolution and explosion of massive stars, Rev. Mod. Phys. **74**, 1015 (2002).

[70] S. Furusawa, H. Togashi, H. Nagakura, K. Sumiyoshi, S. Yamada, H. Suzuki, and M. Takano, A new equation of state for core-collapse supernovae based on realistic nuclear forces and including a full nuclear ensemble, J. Phys. G **44**, 094001 (2017).

[71] K. Sumiyoshi and S. Yamada, Neutrino transfer in three dimensions for core-collapse supernovae. I. Static configurations, Astrophys. J. Suppl. Ser. **199**, 17 (2012).

[72] K. Sumiyoshi, T. Takiwaki, H. Matsufuru, and S. Yamada, Multi-dimensional features of neutrino transfer in core-collapse supernovae, Astrophys. J. Suppl. Ser. **216**, 5 (2015).

[73] Kohsuke Sumiyoshi, Sho Fujibayashi, Yuichiro Sekiguchi, and Masaru Shibata, Properties of neutrino transfer in a deformed remnant of a neutron star merger, Astrophys. J. **907**, 92 (2021).

[74] Hiroki Nagakura, Shun Furusawa, Hajime Togashi, Sherwood Richers, Kohsuke Sumiyoshi, and Shoichi Yamada, Comparing treatments of weak reactions with nuclei in simulations of core-collapse supernovae, Astrophys. J. Suppl. Ser. **240**, 38 (2019).

[75] Akira Harada, Hiroki Nagakura, Wakana Iwakami, Hirotada Okawa, Shun Furusawa, Kohsuke Sumiyoshi, Hideo Matsufuru, and Shoichi Yamada, The Boltzmann-radiation-hydrodynamics simulations of core-collapse supernovae with different equations of state: The role of nuclear composition and the behavior of neutrinos, Astrophys. J. **902**, 150 (2020).

[76] Wakana Iwakami, Hirotada Okawa, Hiroki Nagakura, Akira Harada, Shun Furusawa, Kosuke Sumiyoshi, Hideo Matsufuru, and Shoichi Yamada, Simulations of the early postbounce phase of core-collapse supernovae in three-dimensional space with full Boltzmann neutrino transport, Astrophys. J. **903**, 82 (2020).

[77] H. Nagakura, K. Sumiyoshi, and S. Yamada, Three-dimensional Boltzmann hydro code for core collapse in massive stars I. Special relativistic treatments, Astrophys. J. Suppl. Ser. **214**, 16 (2014).

[78] S. Richers, H. Nagakura, C. D. Ott, J. Dolence, K. Sumiyoshi, and S. Yamada, A detailed comparison of multidimensional Boltzmann neutrino transport methods in core-collapse supernovae, Astrophys. J. **847**, 133 (2017).

[79] Hiroki Nagakura, Retrieval of energy spectra for all flavours of neutrinos from core-collapse supernova with multiple detectors, Mon. Not. R. Astron. Soc. **500**, 319 (2021).

[80] Lucas Johns, Subgrid modeling of neutrino oscillations in astrophysics, arXiv:2401.15247.

[81] Lucas Johns, Thermodynamics of oscillating neutrinos, arXiv:2306.14982.

[82] Hiroki Nagakura, Lucas Johns, and Masamichi Zaizen, BGK subgrid model for neutrino quantum kinetics, Phys. Rev. D **109**, 083013 (2024).

[83] Zewei Xiong, Meng-Ru Wu, Manu George, and Chun-Yu Lin, Robust integration of fast flavor conversions in classical neutrino transport, arXiv:2403.17269.

[84] Hiroki Nagakura and Masamichi Zaizen, Connecting small-scale to large-scale structures of fast neutrino-flavor conversion, Phys. Rev. D **107**, 063033 (2023).

[85] Masamichi Zaizen and Hiroki Nagakura, Simple method for determining asymptotic states of fast neutrino-flavor conversion, Phys. Rev. D **107**, 103022 (2023).

[86] Meng-Ru Wu, Manu George, Chun-Yu Lin, and Zewei Xiong, Collective fast neutrino flavor conversions in a 1D box: Initial conditions and long-term evolution, Phys. Rev. D **104**, 103003 (2021).

[87] Zewei Xiong, Meng-Ru Wu, Manu George, Chun-Yu Lin, Noshad Khosravi Largani, Tobias Fischer, and Gabriel Martínez-Pinedo, Fast neutrino flavor conversions in a supernova: Emergence, evolution, and effects, arXiv:2402.19252.

[88] Masamichi Zaizen and Hiroki Nagakura, Characterizing quasisteady states of fast neutrino-flavor conversion by stability and conservation laws, Phys. Rev. D **107**, 123021 (2023).

[89] Zewei Xiong, Meng-Ru Wu, Sajad Abbar, Soumya Bhattacharyya, Manu George, and Chun-Yu Lin, Evaluating approximate asymptotic distributions for fast neutrino flavor conversions in a periodic 1D box, Phys. Rev. D **108**, 063003 (2023).